ISSN 1674-1056
http://cpb.iphy.ac.cn
http://iopscience.iop.org/cpb
中国物理 B
Chinese Physics
中国物理
Chinese Physics B

Quantum state transfer via a hybrid solid-optomechanical interface

Pei Pei(裴培), He-Fei Huang(黄鹤飞), Yan-Qing Guo(郭彦青), Xing-Yuan Zhang(张兴远), Jia-Feng Dai(戴佳峰)
Citation: Chin. Phys. B . 2018, 27(2): 024203. **doi:** 10.1088/1674-1056/27/2/024203

Journal homepage: http://cpb.iphy.ac.cn; http://iopscience.iop.org/cpb

What follows is a list of articles you may be interested in

Controllable double electromagnetically induced transparency in a closed four-level-loop cavity–atom system

Miao-Di Guo(郭苗迪), Xue-Mei Su(苏雪梅)
Chin. Phys. B . 2017, 26(7): 074207. **doi:** 10.1088/1674-1056/26/7/074207

Adjustable quantum coherence effects in a hybrid optomechanical system

Wen-Qing Xia(夏文清), Ya-Fei Yu(於亚飞), Zhi-Ming Zhang(张智明)
Chin. Phys. B . 2017, 26(5): 054210. **doi:** 10.1088/1674-1056/26/5/054210

Effect of electromagnetic disturbance on thepractical QKD system in the smart grid

Li Fang-Yi, Wang Dong, Wang Shuang, Li Mo, Yin Zhen-Qiang, Li Hong-Wei, Chen Wei, Han Zheng-Fu
Chin. Phys. B . 2014, 23(12): 124201. **doi:** 10.1088/1674-1056/23/12/124201

Heralded linear optical quantum Fredkin gate based on one auxiliary qubit and one single photon detector

Zhu Chang-Hua, Cao Xin, Quan Dong-Xiao, Pei Chang-Xing
Chin. Phys. B . 2014, 23(8): 084207. **doi:** 10.1088/1674-1056/23/8/084207

Phase grating in a doubly degenerate four-level system

Liu Yun, Wang Pu, Peng Shuang-Yan
Chin. Phys. B . 2013, 22(10): 104203. **doi:** 10.1088/1674-1056/22/10/104203

Quantum state transfer via a hybrid solid–optomechanical interface*

Pei Pei(裴培), He-Fei Huang(黄鹤飞)†, Yan-Qing Guo(郭彦青),
Xing-Yuan Zhang(张兴远), and Jia-Feng Dai(戴佳峰)

College of Science, Dalian Maritime University, Dalian 116026, *China*

(Received 24 August 2017; revised manuscript received 25 September 2017; published online 5 January 2018)

We propose a scheme to implement quantum state transfer between two distant quantum nodes via a hybrid solid–optomechanical interface. The quantum state is encoded on the native superconducting qubit, and transferred to the microwave photon, then the optical photon successively, which afterwards is transmitted to the remote node by cavity leaking, and finally the quantum state is transferred to the remote superconducting qubit. The high efficiency of the state transfer is achieved by controllable Gaussian pulses sequence and numerically demonstrated with theoretically feasible parameters. Our scheme has the potential to implement unified quantum computing–communication–computing, and high fidelity of the microwave–optics–microwave transfer process of the quantum state.

Keywords: quantum state transfer, hybrid solid–optomechanical interface, Gaussian pulses

PACS: 42.50.Ex, 42.50.Pq, 42.50.–p, 42.50.Dv **DOI:** 10.1088/1674-1056/27/2/024203

1. Introduction

Quantum state transfer (QST) is an important constituent part of quantum computing (QC), quantum network and quantum communication.[1–6] During QC, quantum state is not only required to be transferred between qubits within the specific computing procedure, but also be transferred between qubits within different steps of computation. When constructing a quantum network, after completing native QC, the quantum state is required to be output from the native quantum node and thus transferred to the remote quantum node.

During native QC, superconducting qubits (SQ)[7,8] coupled to superconducting resonators (SR) such as coplanar waveguide (CPW) resonators[9–11] as the data bus are potential candidates, because the SQ and SR provide the advantages on scalability, controllability, integration, and coherence.[9,12] However, the SQ and SR work in the microwave frequency band, so that the low frequency noise fluctuation can affect the microwave photons, and leads to short coherence times during long distance transmitting.[13] Therefore, microwave photons are not suitable for long distance transmission. Meanwhile the optical photons have good coherence at room temperature, and thus are more suitable for long distance quantum communication and scalable quantum network.[6,14] To combine the advantages of solid qubits for native QC with the advantages of an optical cavity (OC) system for long distance transmission is a crucial task for QST. In previous research, the quantum hybrid interface is a hotspot which contains the solid qubits, the nanomechanical resonator (NAMR) and the OC system. The NAMR is adopted to the medium, which connects to the solid qubits and the OC system, respectively. In previous works, the hybrid interfaces coupled with different physical systems, e.g. ions,[15] cold atoms,[16,17] SRs,[18] and flux qubits[19] are investigated. Yin *et al.*[20] proposed a scheme to realize quantum networking. The SQ is coupled to the SR, which is indirectly coupled to the OC through the optomechanical interface. They reported their measurements to achieve a remote quantum entanglement. In addition, Cernotik *et al.*[21] showed that mechanical oscillators can mediate such coupling and light can be used to measure the joint state of two distant qubits, the measurement provides information on the total spin of two qubits such that entangled qubits states can be post-selected. Most of the predecessors explored the coupling strength of the quantum hybrid interface, and studied in conversion properties of microwave and optics.

In this paper we proposed a scheme to implement QST from an SQ in the native quantum node to the SQ in the remote node. Within each quantum node, SQ is connected to the solid–optomechanical interface which consists of SR, NAMR, and OC. A quantum state is transferred from SQ to optical photons in OC through the hybrid quantum interface, then optical photons leak out from OC and transmit directionally to OC of the remote node. subsequently the quantum state is transferred from the optical photons to SQ of the remote node via the hybrid interface. Our scheme can accomplish the integrative physical process of quantum computing–quantum communication–quantum computing, in addition, it realized the whole conversion of the microwave–optical photons–microwave of the quantum states.

*Project supported by the National Natural Science Foundation of China (Grant No. 11305021) and the Fundamental Research Funds for the Central Universities of China (Grants Nos. 3132017072 and 3132015149).

†Corresponding author. E-mail: huanghefei0789@dlmu.edu.cn

© 2018 Chinese Physical Society and IOP Publishing Ltd

2. Model

The schematic diagram of the whole model is shown in Fig. 1(a), which contains the left unit and the right unit. The quantum state initially encoded on the left unit is transferred to optical photons, and then the optical photons are leaked out from the left unit OC and are transmitted to the right unit OC, finally the photons can be transmitted to the right unit SQ via the hybrid solid–optomechanical interface. In this process, we use a black body absorber[2,22,23] to avoid multiple refections between the two OCs. As shown in Fig. 1(b), within each unit, the superconducting system can be divided into SQ and SR, which couples SQ and SR by capacitively coupling. The NAMR is used as the medium and is coupled with the superconducting system and OC respectively. However the coupling strength, e.g., SQ coupled with SR, SR coupled with NAMR, and NAMR coupled with OC, are typically small, so there are three control pulses used to drive them respectively to enhance their effect.

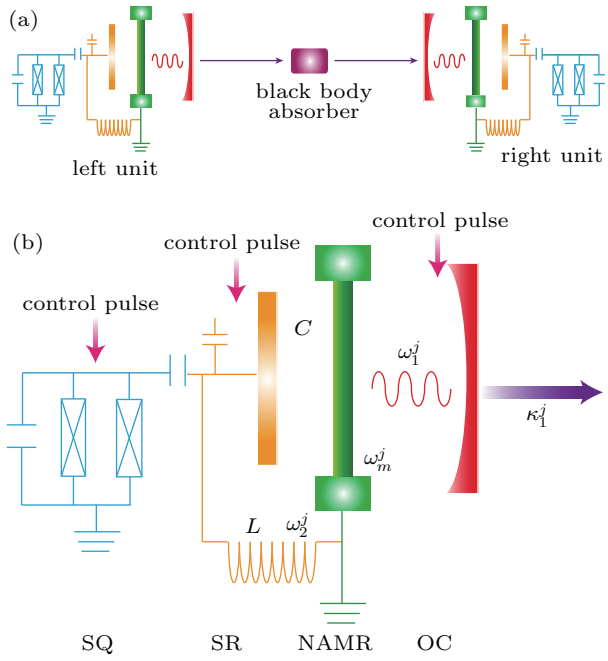


Fig. 1. (color online) (a) Schematic diagram to transfer a quantum state from the left unit to the right unit. The quantum state initially encoded on the left unit is transferred to the right unit, the state can be transferred completely by using adjustable OC leakage rates κ_1^j. A black body absorber can ensure the state transfers in a single direction. (b) Schematic diagram of each unit. The SQ is coupled with the SR by capacitively coupling. The SR and the OC are coupled to the NAMR respectively. The coupling between SQ and SR is driven by a microwave field, meanwhile the SR is driven by a coherent classical field on the microwave band and the OC is driven by an optical field.

The Hamiltonian of each unit has the form $H^j = H_0^j + H_{\rm I}^j + H_{\rm d}^j$ $(j = {\rm l,r})$,[17] where

$$H_0^j = \sum_{i=1,2} \omega_i^j a_i^{\dagger j} a_i^j + \omega_m^j a_m^{\dagger j} a_m^j + \omega_{\rm e}^j \sigma_{\rm ee}^j, \tag{1}$$

$$H_{\rm I}^j = \sum_{i=1,2} g_i^j a_i^{\dagger j} a_i^j \left(a_m^j + a_m^{\dagger j}\right) + g_{\rm c}^j \left(\sigma_{\rm eg}^j + \sigma_{\rm ge}^j\right) \left(a_2^j + a_2^{\dagger j}\right), \tag{2}$$

$$H_{\rm d}^j = \sum_{i=1,2} \left(\frac{\Omega_i^j}{2} {\rm e}^{-{\rm i}\omega_{Li}^j t} + {\rm H.c.}\right) \left(a_i^j + a_i^{\dagger j}\right) + \left(\frac{\Omega'^j}{2} {\rm e}^{-{\rm i}\omega_{L2}^j t} + {\rm H.c.}\right) \left(\sigma_{\rm eg}^j + \sigma_{\rm ge}^j\right), \tag{3}$$

we have set the subscripts of Hamiltonian 0, i, and d as the symbols of free Hamiltonian, interaction Hamiltonian, and driving field, respectively. The superscripts $j = {\rm l,r}$ as the symbols of left unit and right unit, and taken the definition $\sigma_{\mu\nu} = |\mu\rangle\langle\nu|$, a_2^j, a_m^j, a_1^j are the annihilation operators of SR, NAMR, and OC, respectively. $\omega_2^j, \omega_m^j, \omega_1^j$ are the frequencies of SR, NAMR, and OC, respectively. And $\omega_{Li}^j = \omega_m^j - \omega_i^j$. The $g_{\rm c}^j$ is the coupling strength of SQ coupled with SR, and the g_i^j $(i = 1,2)$ is the coupling strength of SR and the OC coupled with NAMR respectively. The control pulses are used to tune SQ to be resonant with SR with $\omega_{\rm e}^j = \omega_2^j$.[2,17] The Ω'^j and Ω_i^j $(i = 1,2)$ are three Rabi frequencies which originate from three control pulses coupled with the system. These Rabi frequencies are used to regulate the relationship between the coupling strengths.

By making use of the rotating-wave approximation,[24–26] the Hamiltonian of the driving field can be obtained in the form of

$$H_{\rm d}^j = \sum_{i=1,2} \left(\frac{\Omega_i^j}{2} a_i^j {\rm e}^{-{\rm i}\omega_{Li}^j t} + {\rm H.c.}\right) + \left(\frac{\Omega'^j}{2} {\rm e}^{-{\rm i}\omega_{L2}^j t} + {\rm H.c.}\right) \left(\sigma_{\rm eg}^j + \sigma_{\rm ge}^j\right). \tag{4}$$

Then we take the rotating frame $H'^j_0 = H_0^j - \sum_{i=1,2} \omega_m^j a^{\dagger j}{}_i a_i^j$, the Hamiltonian under this frame reads

$$\tilde{H}^j = \sum_{i=1,2,m} \omega_m^j a^{\dagger j}{}_i a_i^j + \sum_{i=1,2} g_i^j a_i^{\dagger j} a_i^j \left(a_m^j + a_m^{\dagger j}\right) + \left(g_{\rm c}^j a_2^j {\rm e}^{-{\rm i}\omega_{L2}^j t} + \frac{\Omega'^j}{2} {\rm e}^{-{\rm i}\omega_{L2}^j t} + {\rm H.c.}\right) \left(\sigma_{\rm eg}^j + \sigma_{\rm ge}^j\right) + \left(\frac{\Omega_i^j}{2} a_i^j + {\rm H.c.}\right) + \omega_{\rm e}^j \sigma_{\rm ee}^j. \tag{5}$$

Finally we use steady-state amplitudes of the operators a_i^j, and the operators can be expanded by $\tilde{a}_i^j = a_i^j - c_i^j$, where $c_i^j = \Omega_i^j / 2\omega_m^j$, and under the rotating-wave approximation, the effective Hamiltonian of each unit in the interaction picture[2,20,27] is given by

$$H^j = G^j \left(a_1^{\dagger j} + a_2^{\dagger j}\right) a_m^j + g_{\rm c}^j \sigma_{\rm eg}^j a_2^j + {\rm H.c.}, \tag{6}$$

we take $G^j = g_1^j c_1^j = g_2^j c_2^j$ and the Hamiltonian of the whole system is

$$H = \sum_{j=l,r} G^j \left(a_1^{\dagger j} + a_2^{\dagger j}\right) a_m^j + g_{\rm c}^j \sigma_{\rm eg}^j a_2^j + {\rm H.c.}, \tag{7}$$

and based on the Hamiltonian, the eight Langevin equations[14,28] are taken in the forms as

$$\begin{cases} \dot{a}_1^j = -\mathrm{i}G^j a_m^j - \dfrac{\kappa_1^j}{2}a_1^j + \sqrt{\kappa_1^j}a_{1,\mathrm{in}}^j, \\ \dot{a}_2^j = -\mathrm{i}G^j a_m^j - \mathrm{i}g_\mathrm{c}^j\sigma_\mathrm{ge}^j - \dfrac{\kappa_2^j}{2}a_2^j + \sqrt{\kappa_2^j}a_{2,\mathrm{in}}^j, \\ \dot{a}_m^j = -\mathrm{i}G^j\left(a_1^j + a_2^j\right) - \dfrac{\kappa_m^j}{2}a_m^j + \sqrt{\kappa_m^j}a_{m,in}^j, \\ \dot{\sigma}_\mathrm{ge}^j = \mathrm{i}g_\mathrm{c}^j\sigma_z^j a_2^j - \dfrac{\kappa_\sigma^j}{2}\sigma_\mathrm{ge}^j + \sqrt{\kappa_\sigma^j}\sigma_z^j\sigma_{\mathrm{ge,in}}^j, \end{cases} \tag{8}$$

where $\kappa_\sigma^j, \kappa_2^j, \kappa_m^j$ are the damping rates of SQ, SR, NAMR, respectively. κ_2^j is the leakage rate of OC. Then the input–output relation is used for the left unit OC and the right unit OC, the boundary condition[24] is given by

$$a_{1,\mathrm{in}}^\mathrm{r}(t) = \sqrt{\kappa_1^\mathrm{l}}a_1^\mathrm{l}(t-\tau) - a_{1,\mathrm{in}}^\mathrm{l}(t-\tau), \tag{9}$$

and the classical equations for Langevin equations[2,20,29–32] can be taken in the forms as

$$\begin{cases} \dot{\alpha}_1^\mathrm{l} = -\mathrm{i}G^\mathrm{l}\alpha_m^\mathrm{l} - \dfrac{\kappa_1^\mathrm{l}}{2}\alpha_1^\mathrm{l}, \\ \dot{\alpha}_1^\mathrm{r} = -\mathrm{i}G^\mathrm{r}\alpha_m^\mathrm{r} - \dfrac{\kappa_1^\mathrm{r}}{2}\alpha_1^\mathrm{r} + \sqrt{\kappa_1^\mathrm{l}\kappa_1^\mathrm{r}}\alpha_1^\mathrm{l}, \\ \dot{\alpha}_2^j = -\mathrm{i}G^j\alpha_m^j - \mathrm{i}g_\mathrm{c}^j\vartheta_\mathrm{ge}^j - \dfrac{\kappa_2^j}{2}\alpha_2^j, \\ \dot{\alpha}_m^j = -\mathrm{i}G^j\left(\alpha_1^j + \alpha_2^j\right) - \dfrac{\kappa_m^j}{2}\alpha_m^j, \\ \dot{\vartheta}_\mathrm{ge}^j = \mathrm{i}g_\mathrm{c}^j\sigma_z^j\alpha_2^j - \dfrac{\kappa_\sigma^j}{2}\vartheta_\mathrm{ge}^j, \end{cases} \tag{10}$$

where α_i and $\vartheta_{\mu\nu}$ are the classical forms for a_i and $\sigma_{\mu\nu}$ respectively. Under the classical Langevin equations, the steady-state of each mode is given by

$$\begin{cases} 0 = -\mathrm{i}G^\mathrm{l}\left\langle\alpha_m^\mathrm{l}\right\rangle - \dfrac{\kappa_1^\mathrm{l}}{2}\left\langle\alpha_1^\mathrm{l}\right\rangle, \\ 0 = -\mathrm{i}G^\mathrm{r}\left\langle\alpha_m^\mathrm{r}\right\rangle - \dfrac{\kappa_1^\mathrm{r}}{2}\left\langle\alpha_1{}^\mathrm{r}\right\rangle + \sqrt{\kappa_1^\mathrm{l}\kappa_1^\mathrm{r}}\left\langle\alpha_1^\mathrm{l}\right\rangle, \\ 0 = -\mathrm{i}G^j\left\langle\alpha_m^j\right\rangle - \mathrm{i}g_\mathrm{c}^j\left\langle\vartheta_\mathrm{ge}^j\right\rangle - \dfrac{\kappa_2^j}{2}\left\langle\alpha_2^j\right\rangle, \\ 0 = -\mathrm{i}G^j\left(\left\langle\alpha_1^j\right\rangle + \left\langle\alpha_2^j\right\rangle\right) - \dfrac{\kappa_m^j}{2}\left\langle\alpha_m^j\right\rangle, \\ 0 = \mathrm{i}g_\mathrm{c}^j\sigma_z^j\left\langle\alpha_2^j\right\rangle - \dfrac{\kappa_\sigma^j}{2}\left\langle\vartheta_\mathrm{ge}^j\right\rangle, \end{cases} \tag{11}$$

the form of σ_z^j by solving equations[24] is shown as

$$\sigma_z^j = -\frac{\kappa_1^j\kappa_\sigma^j + \kappa_2^j\kappa_\sigma^j + \kappa_1^j\kappa_2^j\kappa_\mathrm{m}^j\kappa_\sigma^j/4G^{j2}}{4g_\mathrm{c}^{j2} + \kappa_1^j\kappa_m^j g_\mathrm{c}^{j2}/G^{j2}}. \tag{12}$$

While the quantum state is transferred from the left unit OC to the right unit OC, we define $a_1^\mathrm{l}(0) = 1$, $a_1^\mathrm{r}(0) = 0$, $g_\mathrm{c}^\mathrm{l} = g_\mathrm{c}^\mathrm{r} = G^\mathrm{l} = G^\mathrm{r} = 0$, by solving the Langevin equations, $a_1^\mathrm{r}(t)$ is taken as the form[2,29]

$$\begin{aligned} a_1^\mathrm{r}(t) &= a_1^\mathrm{r}(0)\exp\left(\frac{-\kappa_1^\mathrm{r}t}{2}\right) + a_1^\mathrm{l}(0)\sqrt{\kappa_1^\mathrm{r}} \\ &\quad\times\int_0^t \mathrm{d}t'\sqrt{\kappa_1^\mathrm{l}(t')}\exp\left(-\frac{\kappa_1^\mathrm{r}(t-t')}{2}\right) \\ &\quad\times\exp\left(-\frac{1}{2}\int_0^{t'}\mathrm{d}t''\kappa_1^\mathrm{l}(t')\right), \end{aligned} \tag{13}$$

and the state transfer efficiency can be defined as

$$\begin{aligned} \eta &= \sqrt{\kappa_1^\mathrm{r}}\cdot\int_0^t \mathrm{d}t'\sqrt{\kappa_1^\mathrm{l}(t')}\exp\left(-\frac{\kappa_1^\mathrm{r}(t-t')}{2}\right) \\ &\quad\times\exp\left(-\frac{1}{2}\int_0^{t'}\mathrm{d}t''\kappa_1^\mathrm{l}(t')\right), \end{aligned} \tag{14}$$

this can be rewritten as

$$\eta(A,A',t) = \sqrt{\kappa_1^\mathrm{r}}\cdot\int_0^t \mathrm{d}t'\sqrt{A'}\exp\left(-\frac{\kappa_1^\mathrm{r}(t-t')}{2}\right)\mathrm{e}^{-A/2}. \tag{15}$$

According to the form of Euler–Lagrange formalism, the leakage rates are obtained by solving $\partial\eta/\partial A = \mathrm{d}(\partial\eta/\partial A')/\mathrm{d}t$ is given by

$$\kappa_1^\mathrm{l}(t) = \frac{\kappa}{2\mathrm{e}^{\kappa(t_m-t)}-1}, \tag{16}$$

$$\kappa_1^\mathrm{r}(t) = \frac{\kappa}{2\mathrm{e}^{\kappa(t-t_m)}-1}, \tag{17}$$

where κ is the maximum value of OCs. And the t_m guarantees the directionality of photons transmission, when $0 \le t \le t_m$, and then $\kappa_1^\mathrm{l}(t) \le \kappa_1^\mathrm{r}(t)$, so the quantum state is stored in the left unit OC, meanwhile when $t \ge t_m$, the quantum state is stored in the right unit OC. This operation can be shown by choosing a time-dependent switching which is between the OC and the transmission line.[2,6]

The model of the QST has eight parts, under the influence of coupling strengths, the QST between the parts is bidirectionally. If the state is transferred, it returns to the previous part, we call it inverse flow, which can damage the transfer efficiency. To avoid it, we investigate the appropriate values of the t_m and G^j in the next sections.

3. The QST by the hybrid solid–optomechanical interface

Here we consider the QST from the left unit to the right unit, and demonstrate the results of transfer in three parts. In order to be closed to reality, we adopt parameters verified in theories and experiments as $\kappa/2\pi = 215$ kHz, $\kappa_2^\mathrm{l}/2\pi = \kappa_2^\mathrm{r}/2\pi = 1$ kHz, $\kappa_m^\mathrm{l}/2\pi = \kappa_m^\mathrm{r}/2\pi = 140$ Hz and $\kappa_\sigma^\mathrm{l}/2\pi = 5$ kHz,[2,20] and consider $\kappa_\sigma^\mathrm{r}/2\pi = 0$ to investigate the quantum state to be transferred to the right unit SQ.

3.1. Energy transfer efficiency of the hybrid quantum interface

In this section, the energy transfer capability of the hybrid quantum interface is investigated, the energy begins to transfer from the left unit SR, then to the left NAMR, the left OC, the right OC, and the right NAMR successively, finally transferring to the right unit SR. We set $g_c^l = g_c^r = 0$ to avoid SQ participating in the transfer process and set the initial value as $\alpha_2^l(0) = 1$, $\vartheta_{ge}^j(0) = \alpha_m^j(0) = \alpha_1^j(0) = \alpha_2^r(0) = 0$, and characterize the capability by the energy transfer efficiency

$$E = |\alpha_2^r(t)|^2 / \left|\alpha_2^l(0)\right|^2.$$

In order to facilitate the calculation, we consider $G^l = G^r = G = g_i^j \Omega_i^j / 2\omega_m^j$ by adjusting coupling strengths g_i $(i = 1,2)$ and Rabi frequencies Ω_i^j, then choose the appropriate value of t_m to achieve a high energy transfer efficiency, here the efficiency is discussed as a function of the G/κ for different t_m. The results are shown in Fig. 2. In each figure, we select different procedure times t as $t \cdot \kappa = 25$, $t \cdot \kappa = 35$, and $t \cdot \kappa = 45$. In different figures, we set $t_m \cdot \kappa = 17.55$ and 4.7 in Figs. 2(a) and 2(b) respectively.

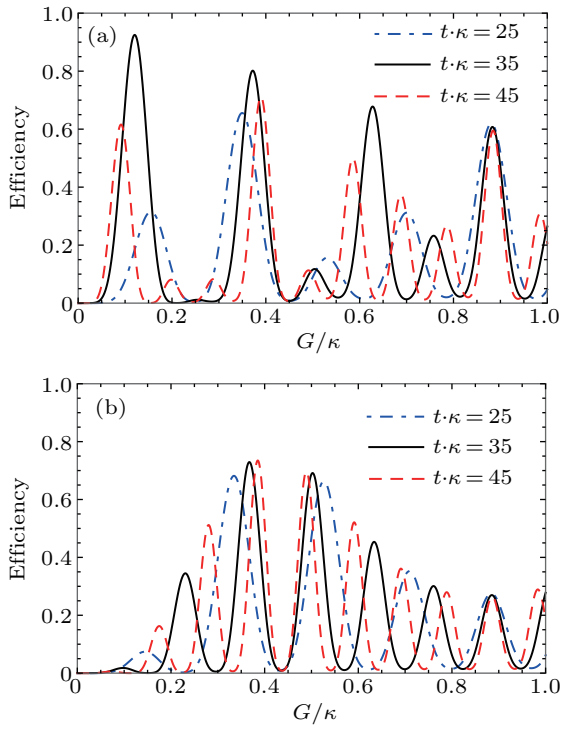


Fig. 2. (color online) The energy transfer efficiencies for the hybrid quantum interface under the different t_m as the function of G/κ. In Figs. 2(a) and 2(b) we set $t_m \cdot \kappa = 17.55$ and $t_m \cdot \kappa = 4.7$ respectively, and the efficiency for the different procedure times $t \cdot \kappa = 25$ (dash-dotted, blue), $t \cdot \kappa = 35$ (solid, black), and $t \cdot \kappa = 45$ (dashed, red).

Comparing Fig. 2(a) with Fig. 2(b), t_m influences the maximum efficiency, since figure 2(a) has a longer t_m, the energy will be transferred to the right unit SR with the procedure time we select. Meanwhile the t_m in Fig. 2(b) is shorter, so the photons will be leaked prematurely and the energy has been transferred to the right unit SR before the times ($t \cdot \kappa = 25$, 35, and 45) we selected, then the energy will emerge with inverse flow and cause the peak value of the efficiency to decrease. Moreover, the maximum efficiencies in Figs. 2(a) and 2(b) correspond to different coupling strengths, the longer t_m causes the maximum efficiency with a weaker coupling strength. Because when t_m is longer, the optical photons have been stored in the left unit OC before photons transmission by leaking, and it does not need a larger coupling strength to accelerate the energy transferring to the left unit OC, so that the longer t_m provides the prerequisite for reducing the coupling strength. In each figure, the efficiency presents quasi-periodic decreasing as a function of the coupling strength G. The reason is that the coupling strength increases by double emerging the maximum effect of the inverse flow which causes the minimum energy transfer efficiency. When the coupling strength continues to increase, the inverse flow will occur in the six parts of the model, and disperses the energy in all parts of the transfer route, so the peak values of the efficiency will decrease with the coupling strength increasing periodically.

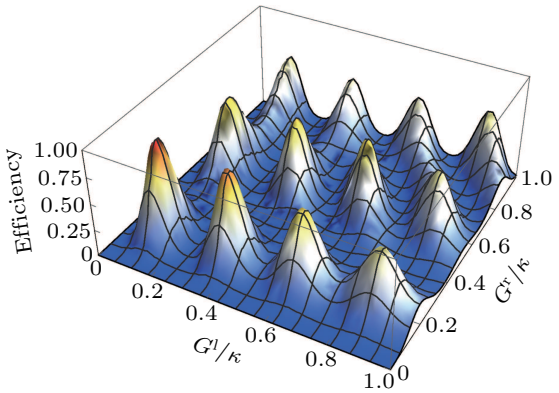


Fig. 3. (color online) The efficiency of the energy transfer from the left unit SR to the right unit SR for $t \cdot \kappa = 28.5$ as a function of G^l/κ and G^r/κ. The parameter is taken as $t_m \cdot \kappa = 17.55$. The maximum efficiency is 97.5% under the coupling strengths $G^l/\kappa = 0.12$ and $G^r/\kappa = 0.2$.

According to the result in Fig. 2, in order to achieve a high efficiency, we adjust and fix the parameters as $t_m \cdot \kappa = 17.55$ and $t \cdot \kappa = 28.5$. Without loss of generality, the plot of the energy transfer efficiency is investigated as a function of the two coupling strengths G^l and G^r, as shown in Fig. 3. There are multiple peaks appearing as the coupling strengths increase, the optimum efficiency $\sim 97.5\%$ is obtained by two coupling strengths $G^l/\kappa = 0.12$ and $G^r/\kappa = 0.2$. These parameters will be used in the next sections. Notice that the peak values have different numbers as the functions of G^j, there are four peak values within the range of G^l, meanwhile the range of G^r has three. That is because the G^l influences the whole process of the transfer, while the G^r just influences the process after t_m when the energy has been transferred to the right unit.

3.2. Occupation number transfer for the hybrid quantum interface

The occupation number transfer of the hybrid quantum interface is investigated in this section, the transfer route of the model has six parts ∼left SR–left NAMR–left OC–right OC–right NAMR-right SR, and the occupation numbers are used to show the QST between the six parts. The initial value is taken as $\alpha_2^{\rm l}(0)=1$, $\vartheta_{\rm ge}^{j}(0)=\alpha_m^{j}(0)=\alpha_1^{j}(0)=\alpha_2^{\rm r}(0)=0$, and to achieve the maximum efficiency, the parameters are taken as $t_m\cdot\kappa=17.55$, $G^{\rm l}/\kappa=0.12$, $G^{\rm r}/\kappa=0.2$, the coupling strengths of the SQ are not considered. The results of numerical simulation are obtained by Eqs. (10).

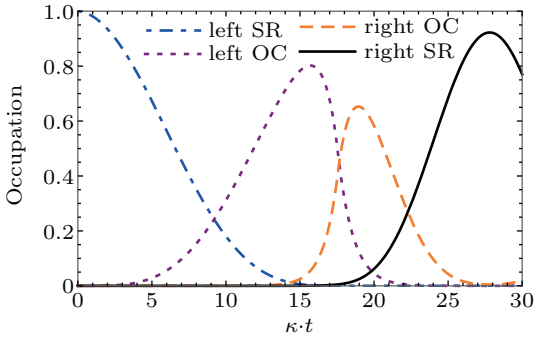


Fig. 4. (color online) Shape of occupation numbers for the four modes as a function of procedure time $t\cdot\kappa$, the parameters are taken as $t_m\cdot\kappa=17.55$, $G^{\rm l}/\kappa=0.12$, $G^{\rm r}/\kappa=0.2$. The dash–dotted blue curve, the dotted purple curve, the dashed orange curve, and the solid black curve are the left unit SR, the left unit OC, the right unit OC, and the right unit SR, respectively.

The plot of the occupation numbers is shown in Fig. 4, there are four occupation numbers to be demonstrated, which can show the quantum state in the beginning and the ending of the model, it is further shown that the optical photons are stored in the left unit OC and leaked out to the right unit OC. The initial occupation numbers are stored in the left unit SR, and go through NAMR and OC in the left unit, then leak out and go to OC-NAMR in the right unit, finally they will be stored in the right unit SR.

The occupation numbers of the right unit SR in Fig. 4 can exceed 0.9, however the occupation numbers of OCs are not close to 1 during the transfer process. The reason is as follows. One cannot store all the occupation numbers into OC and then transfer them completely to the right unit, since the coupling strengths are considered as constants in this case. Thus, while the occupation number is transferring to the right unit, the continuous couplings between SR–NAMR–OC result in the occupation number transferring back to the left NAMR, and even further to SR. We can note that the efficiency for both the two OCs is higher than that for the right SR. When the quantum state is transferring from the OCs to the right SR, the inverse flow causes the transfer process to have two directions, one can transfer the state to the right SR, the other will transfer the state back to the left NANR and other parts within the left unit. To avoid this inverse flow, the t_m is adjusted in order that once the occupation number begins to be stored into the OC, it is transferred to the right unit simultaneously. We can adjust the t_m as an optimal value to achieve the maximum efficiency, if t_m is larger than the optimal value, the optical photons will be stored in the left unit OC and emerge in the inverse flow, if t_m is less than the optimal value, the photons have no time to be transmitted to the left unit OC, so the OC does not have enough optical photons to be leaked out.

3.3. QST from the left unit SQ to the right unit SQ

Here we discuss the QST from the left unit SQ to the right unit SQ, the SQs are coupled to SRs of the hybrid quantum interface by coupling strengths $g_{\rm c}^{j}$. In this section, the model includes eight parts. The longer transfer route causes the subsystems increasing and the numbers of coupling strengths increase to four ($g_{\rm c}^{j}$ and G^{j}) simultaneously, therefore the inverse flow is aggravated. Furthermore, QST in the longer transfer route will take more procedure time, thus the efficiency is prone to be decreased by damping. This effect is manifested in Fig. 5(a), the quantum state is transferred within eight parts of the whole system by using the continuous pulses, and we set the optimal value of the coupling strengths $G^{\rm l}/\kappa=g_{\rm c}^{\rm l}/\kappa=0.12$, $G^{\rm r}/\kappa=g_{\rm c}^{\rm r}/\kappa=0.2$. The efficiency for each part is lower than that for the corresponding parts in Fig. 4.

The reason for causing the inverse flow is that the coupling strengths are induced by continuous pulses. To avoid it, the control pulse should provide a strength to couple conjoint parts when the quantum state needs to be passed forward, and once the quantum state has been transferred to the next part, the control pulse should be cut off and the coupling strength vanishes simultaneously. Thus a controllable coupling strength to set the trigger time and the duration of the coupling strength is essential. In order to restrict the influence of the damping, the coupling strength can also be controlled to shorten the procedure time by hurrying the trigger time. So the Gaussian pulses are the candidates to control the coupling strengths and take the forms as

$$g_{\rm c}^{\rm l}(t)=g_0^{\rm l}\times\exp\left[-\frac{\left(t-\frac{1}{2}t_{d1}\right)^2}{2\times t_{w1}^2}\right], \tag{18}$$

$$G^{\rm l}(t)=G_0^{\rm l}\times\exp\left[-\frac{\left(t-\frac{1}{2}t_{d2}\right)^2}{2\times t_{w2}^2}\right], \tag{19}$$

$$g_{\rm c}^{\rm r}(t)=g_0^{\rm r}\times\exp\left[-\frac{\left(t-\frac{1}{2}t_{d3}\right)^2}{2\times t_{w3}^2}\right], \tag{20}$$

$$G^{\rm r}(t)=G_0^{\rm r}\times\exp\left[-\frac{\left(t-\frac{1}{2}t_{d4}\right)^2}{2\times t_{w4}^2}\right]. \tag{21}$$

In the expression of the Gaussian pulses, g_0^{j} and G_0^{j} are the controllable amplitudes which take the forms $G_0^{j}=g_i^{j}\Omega_i^{j}/2\omega_m^{j}$

and $g_0^j = \omega_m \Omega'^j / \Omega_2^j$,[2,20] where Ω_i^j and Ω'^j are the controllable parameters by applying the driving fields. t_{di} and t_{wi} ($i = 1,2,3,4$) are the peak times and the pulse widths of the four Gaussian pulses Eqs. (18)–(21) respectively. These parameters influence the coupling strengths and procedure times during the QST, only the appropriate parameters of Gaussian pulses [shown in Fig. 5(c)] can avoid the inverse flow and achieve the maximum efficiency.

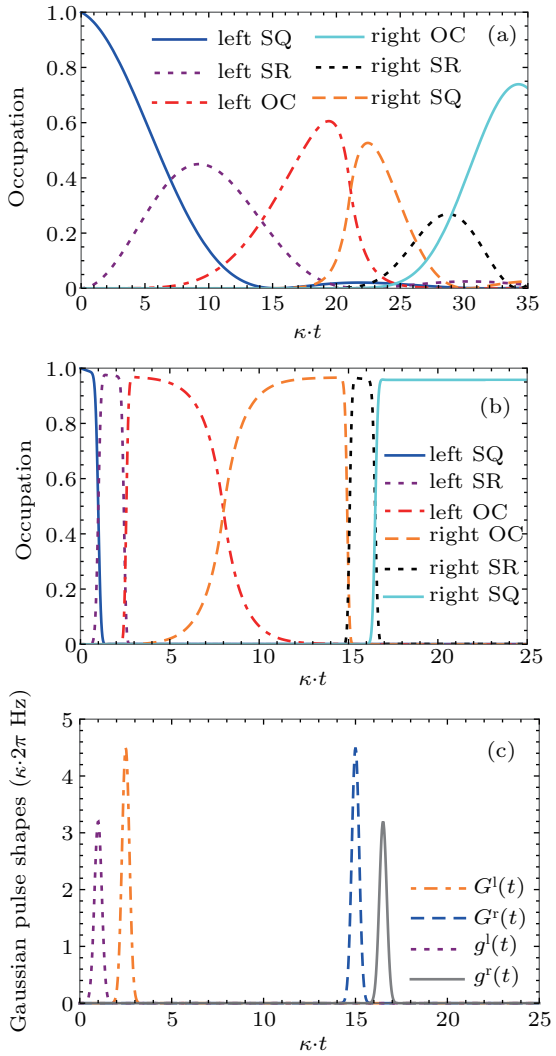


Fig. 5. (color online) (a) and (b) Occupation numbers for the six modes. The coupling strength of panel (a) is induced by the continuous pulses, meanwhile (b) is the Gaussian pulses, we set $t_m \cdot \kappa = 21$ and 8 in panels (a) and (b) respectively. The quantum state is initially encoded on the left unit SQ (solid, blue) is transferred to the left unit SR (dotted, purple), and the left unit OC (dash-dotted, red) by using coupling strengths g_c^l and G^l, then the photons radiate to the right unit OC (dashed orange curve), finally the photons are transmitted to the right unit SR (dotted, black) and the right unit SQ (solid, cyan) by utilizing coupling strengths G^r and g_c^r respectively. (c) The shapes of four Gaussian pulses $g_c^l(t)$ (dotted, black), $G^l(t)$ (dash–dotted, brown), $G^r(t)$ (thick-dashed, gray) and $g_c^r(t)$ (dashed, green). The parameters are taken as $g_0^l/\kappa = 3.2$, $G_0^l/\kappa = 4.5$, $G_0^r/\kappa = 4.5$, $g_0^r/\kappa = 3.2$, $t_{d1} \cdot \kappa = 2$, $t_{d2} \cdot \kappa = 5$, $t_{d3} \cdot \kappa = 30$, $t_{d4} \cdot \kappa = 33$, $t_{w1} \cdot \kappa = t_{w2} \cdot \kappa = t_{w3} \cdot \kappa = t_{w4} \cdot \kappa = 0.2$.

In this section we demonstrate the QST by using occupation number and consider the initial conditions as $\vartheta_{ge}^l(0) = 1$, $\alpha_1^j(0) = \alpha_m^j(0) = \alpha_2^j(0) = \vartheta_{ge}^r(0) = 0$. As shown in Figs. 5(a) and 5(b), the quantum state is encoded on the left unit SQ initially, then the state is transferred to the left unit SR through Gaussian pulse $g_c^l(t)$ and encoded on the microwave photons. After that, the quantum state is transferred to the optical photons in the left unit OC by applying the Gaussian pulse $G^l(t)$, in this part the optical photons leak out and is transmitted to the OC in the right unit, and then the optical photons are transferred back to microwave photons and are transmitted to the right unit SR by utilizing the Gaussian pulse $G^r(t)$. Finally the state is encoded on the right unit SQ by using the Gaussian pulse $g_c^r(t)$. Figure 5(c) is the schematic diagram of the Gaussian pulses, the time interval between $g_c^j(t)$ and $G^j(t)$ is small, since narrowing the distance between $g_c^j(t)$ and $G^j(t)$ can reduce the procedure time and weaken the influence of the damping. Notice that the distance between $G^l(t)$ and $G^r(t)$ is not controlled within a small range. The reason is as follows: during the time interval between $G^l(t)$ and $G^r(t)$, the optical photons are required to be leaked out from the left unit OC and into the right unit OC, so the optical photons need enough procedure time to transfer sufficiently. Thus we set the time interval between t_{d2} and t_{d3} as $12.5/\kappa$ to ensure the transfer efficiency between the OCs. In the continuous pulses situation [shown in Fig. 5(a)], the efficiency is close to 75%, meanwhile the efficiency as shown in Fig. 5(b) can be nearly 95% in the Gaussian pulses situation.

We call the process where the quantum state can be transferred from the left unit to the right unit the "writing protocol", and the reverse process, the "reading protocol", can also be realized to transfer the quantum state from the right unit to the left unit. The Gaussian pulses are applied in the reverse order, the state initially stored in the right unit SQ is transferred to the right unit SR by Gaussian pulse $g_c^r(t)$, and then passed to the hybrid quantum interface by using $G^r(t)$ and $G^l(t)$ successively, finally the $g_c^l(t)$ is used to make the quantum state transfer to SQ in the left unit.

4. Summary and prospect

In summary, we have described a blueprint of the QST based on the hybrid solid–optomechanical interface. The transfer route consists of SQ–SR–NAMR–OC in the native quantum node and OC–NAMR–SR–SQ in the remote quantum node, we call the structure which contains the SR–NAMR–OC the "hybrid solid–optomechanical interface". When the quantum states are within the interface, the states will be transferred from the microwave photons to the optical photons and are stored in OC. We adjust t_m to control OC to leak out the optical photons and to transfer the photons to the remote quantum node. The significance of the scheme is uni-

fied microwave photons–optical photons–microwave photons transfer process of the quantum states.

According to this model, the further research can proceed as follows. In order to transmit the optical photons more controllably, the optical fiber can be used between OCs,[33] and we can set the trigger time to couple the optical fiber with OCs to achieve an optimal transfer efficiency. Moreover, we can also investigate the QST based on other solid qubits, NV center,[34] flux qubits,[35] and ions[36] to promise stability and controllability, which are other candidates for the QST.

Acknowledgments

Huang H F acknowledges Gao Yi-Bo, Yin Zhang-Qi and Zhang Zuo-Yuan for valuable discussions.

References

[1] Neto G D D, Andrade F M, Montenegro V and Bose S 2016 *Phys. Rev. A* **93** 062339
[2] Sete E A and Eleuch H 2015 *Phys. Rev. A* **91** 032309
[3] Pei P, Huang H F, Guo Y Q and Song H S 2016 *Chin. Phys. Lett.* **33** 020301
[4] Li X H 2016 *Acta Phys. Sin.* **65** 030302 (in Chinese)
[5] Ma H Y, Qin G Q, Fan X K and Chu P C 2015 *Acta Phys. Sin.* **64** 160306 (in Chinese)
[6] Razavi M and Shapiro J H 2006 *Phys. Rev. A* **73** 042303
[7] Blais A, Huang R S, Wallraff A, Cirvin M S and Schoelkopf R J 2004 *Phys. Rev. A* **69** 062320
[8] Blais A, Gambetta J, Wallraff A, Schuster D I, Cirvin M S, Devoret M H and Schoelkopf R J 2007 *Phys. Rev. A* **75** 032329
[9] Xiang Z L, Ashhab S, You Z Q and Franco N 2013 *Rev. Mod. Phys.* **85** 623
[10] Rabl P, Cappellaro P, Dutt M V G, Jiang L, Maze J R and Lukin M D 2009 *Phys. Rev. B* **79** 041302
[11] Das S E, Vincent E and Faez S 2017 *Phys. Rev. Lett.* **118** 140501
[12] Hofheinz M, *et al.* 2008 *Nature* **454** 7202
[13] Manuchargan V E, Koch J, Glazman L I and Devoret M H 2009 *Science* **326** 113
[14] Aspelmeyer, Markus, Kippenberg, Tobias J, Marquard and Florian 2014 *Rev. Mod. Phys.* **86** 1391
[15] Bhattacherjee A B 2016 *Int. J. Theor. Phys.* **55** 1944
[16] Ranjit G, Montoga C and Geraci A A 2015 *Phys. Rev. A* **91** 013416
[17] Zhong H *et al.* 2017 *Rev. Sci. Instrum.* **88** 023115
[18] Johansson J R, Johansson G and Nori F 2014 *Phys. Rev. A* **90** 053833
[19] Xiong W *et al.* 2015 *Phys. Rev. A* **92** 032318
[20] Yin Z Q, Yang W L, Sun L and Duan L M 2015 *Phys. Rev. A* **91** 012333
[21] Cernotik O and Hammerer K 2016 *Phys. Rev. A* **94** 012340
[22] Kim D S, Cho J W, Park K, Kim Y S and Kim S K 2017 *Curr. Appl. Phys.* **17** 1015
[23] Aspelmeyer, Markus, Kippenberg, Tobias J, Marquard, Florian 2014 *Cavity Optomechanics* (Berlin: Springer)
[24] Yin Z Q and Han Y J 2009 *Phys. Rev. A* **79** 024301
[25] Wang Y D and Clerk A A 2012 *Phys. Rev. Lett.* **108** 153603
[26] Tian L 2012 *Phys. Rev. Lett.* **108** 153604
[27] Walls D F and Milburn G J 2007 *Quantum Optics* (Berlin: Springer)
[28] Warwick P, Bowen, Gerard J and Milburn 2016 *Quantum Optomechanics* (U.S.: CRC)
[29] Jahne K, Yurke B, and Gavish U 2007 *Phys. Rev. A* **75** 010301
[30] Korotkov A N 2011 *Phys. Rev. B* **84** 014510
[31] Sete E A, Mlinar E and Korotkov A K 2015 *Phys. Rev. B* **91** 144509
[32] James D F V and Jerke J 2007 *Can. J. Phys.* **85** 625
[33] Choi H, Park M, Elliott D S and Oh K 2017 *Phys. Rev. A* **95** 053817
[34] Pei P, Zhang F Y, Li C and Song H S 2011 *Phys. Rev. A* **84** 042339
[35] Chen Q, Yang W L and Feng M 2012 *Phys. Rev. A* **86** 022327
[36] Shi. J F, Ge B J and Wang D X 2016 *Int. J. Theor. Phys.* **55** 2928